Nonlinear Dynamics (2026) 114:1163
https://doi.org/10.1007/s11071-026-13068-5

RESEARCH

Geometric optimization of a single-particle impact damper for mode-specific vibration suppression in multi-storey structures

Muhammad Ayaz Akbar[1,3] · Emiliano Rustighi[2] · Muhammad Gulzari[3] · Chengzhen Yin[1] · Qinghua Qin[1]

Received: 25 April 2026 / Revised: 28 August 2026 / Accepted: 6 September 2026 / Published online: 18 September 2026
© The Author(s), under exclusive licence to Springer Nature B.V. 2026

Abstract

This study introduces a Tuned Single-Particle Impact Damper (TSPID) developed for mode-selective vibration suppression in multi-degree-of-freedom (MDOF) structures. While particle impact dampers are typically recognized for their broadband effectiveness around the fundamental resonant frequency, their ability to achieve mode-selective attenuation in resonant modes of MDOF structures has received comparatively limited investigation. This work combines numerical parametric studies with experimental validation on a scaled five-story shear-type building to show that a single geometric parameter, the clearance gap, enables effective and robust mode-selective suppression. Three performance metrics are used: modal $H_{i,\infty}$ norm (peak response at each resonance i), total vibration energy, and inter-storey drift (ISD). When optimized for the first mode, the TSPID achieves average reductions of 95% in vibration energy, 93% in ISD, and 86% in modal $H_{1,\infty}$ norm across all floors. When it is optimized for the second mode, the corresponding reductions remain substantial (85% in vibration energy, 79% in ISD, and 66% in modal $H_{2,\infty}$ norm). Performance is largely insensitive to the choice of impact-surface material (polyurethane versus polyethylene foam, with differences below 5% across all metrics), confirming that energy dissipation is governed primarily by impact dynamics rather than exact restitution or stiffness values. Numerical impact sequencing analysis further reveals that effective suppression coincides with approximately two regular impacts per excitation cycle at sufficient mean impact velocity, supporting the role of impact sequencing and impact velocity in the observed mode-selective suppression. The normalized clearance D is identified as a physically meaningful design parameter that inherently accounts for the amplitude-clearance interaction governing impact effectiveness. These results establish a practical, geometrically simple design framework for mode-targeted vibration control. By bridging general particle-damper effectiveness and mode-selective suppression, the TSPID offers high efficacy, low cost, and inherent robustness, making it particularly attractive for resonant-dominated civil and mechanical structures.

Keywords Tuned particle damper · Single-particle impact damper · MDOF structure · Targeted modal damping · Passive vibration control · Inter-storey drift

1 Introduction

The increasing demand for structural reliability under dynamic loads such as wind [1], impacts [2, 3], and earthquakes [4–6] has fuelled decades of research into vibration control systems. Although passive, active, and hybrid methods [7–11] have advanced considerably, passive dampers remain especially attractive owing to their simplicity, cost-effectiveness, and independence from external power [12, 13]. Among these, particle impact dampers (PIDs) [14] stand out as effective solutions that dissipate energy through inelastic collisions and

✉ Muhammad Gulzari
muhammad.gulzari@ucd.ie

[1] Institute of Advanced Interdisciplinary Technology, Shenzhen MSU-BIT University, Longgang District, Shenzhen, Guangdong, China

[2] Department of Industrial Engineering, University of Trento, Trento, Italy

[3] School of Civil Engineering, University College Dublin, Dublin, Belfield, Dublin 4, Dublin, Ireland

momentum transfer in terms of simpler design and installation, effectiveness in harsh environmental conditions, and cost effectiveness [15].

The foundational analytical framework for impact damping in single-degree-of-freedom (SDOF) systems was established in the seminal works of Masri [16–21]. These studies provided exact steady-state solutions and stability criteria that have been widely adopted. Subsequent research extended the concept to multi-degree-of-freedom (MDOF) systems [22] and interpreted it within the broader context of vibro-impact nonlinear energy sinks (NES) [23–26] for broadband vibration suppression and to practical single-particle impact dampers (SPIDs) whose performance can be adjusted through straightforward geometric modifications [27–34]. In recent years the field has seen rapid progress, including data-driven and AI-based optimization methods [35–37], adaptive tuned particle dampers [38–44], non-packed granular configurations [45–47], and applications to vortex-induced vibration [48, 49], wind-turbine blades [50–52], and seismic protection of multi-story buildings [53–55].

Previous studies have examined the influence of clearance in impact dampers for multi-degree-of-freedom systems. Li and Darby [56–59] conducted systematic experimental investigations on buffered impact dampers in MDOF structures and observed that the effect of clearance can be unpredictable, particularly for higher modes. More recently, Geng et al. [60] demonstrated that each resonance mode can possess a different optimal clearance. These works highlight the mode-dependent nature of optimal clearance in impact dampers. Despite these advances, experimental verification of purely geometric, mode-selective suppression a single-particle impact damper in multi-storey structures remains limited. While the previous research highlighted the mode-dependent influence of clearance, systematic experimental demonstration of preferential suppression of individual modes through clearance adjustment alone, together with robustness to material parameters (coefficient of restitution and contact stiffness), has not been fully explored. Masri and Caffrey [61] investigated a pounding vibration absorber on an MDOF system, consisting of a classical tuned mass damper with motion-limiting stops. In contrast, the proposed Tuned Single-Particle Impact Damper (TSPID) relies solely on impact dynamics, with its vibration suppression performance optimized primarily through geometric adjustment of the clearance gap. This approach eliminates the need for precise stiffness matching and offers a simpler implementation for achieving mode-selective vibration suppression.

The present work provides experimental validation of a TSPID for mode-specific vibration suppression in MDOF systems. Using systematic geometric optimization, the device demonstrates preferential attenuation of individual modes. A five-degree-of-freedom (5-DOF) shear-type building model was chosen because it is a representative, well-studied configuration that clearly separates the first two modes and allows direct evaluation of inter-storey drift, an important serviceability metric. The study systematically examines how the geometric parameters of the TSPID, primarily the clearance gap, influence vibration mitigation performance across different modes. This approach enables a quantitative multi-metric evaluation, including modal $H_{i,\infty}$ norm attenuation (i.e., peak response reduction at targeted resonances rather than the conventional broadband worst-case norm), vibration energy dissipation, and inter-storey drift mitigation. The results provide practical guidelines for configuring TSPIDs for mode-selective vibration suppression and clarify the trade-offs between suppression effectiveness and robustness. The physical mechanism underlying mode selectivity is further examined through numerical impact sequencing analysis, which characterises the number of impacts per excitation cycle and the mean impact velocity at each modal frequency, providing further insight into the impact behavior associated with the observed mode-selective suppression. The work contributes a practical pathway from general PID effectiveness to mode-selective damper design through geometric optimization.

The remainder of this paper is structured as follows. Section 2 introduces the theoretical model and experimental methodology. Section 3 reports parametric analyses and experimental results, evaluating TSPID performance under various configurations. Section 4 summarizes the key findings, discusses implications for structural vibration control, and suggests future research directions.

2 Methodology

This section outlines the research methodology. First, a theoretical model of the SPID coupled to a 5-DOF structure is developed. Next, a parametric analysis is performed to examine the effects of key design parameters on the suppression of multiple vibration modes. Finally, an experimental setup is constructed to validate the numerical findings.

2.1 Theoretical model

The five-story structure is modelled as a 5-DOF shear building (Fig. 1a). Each floor has mass $m = 1.71\text{kg}$ and inter-storey stiffness $k = 3368.5\text{N/m}$. A base excitation $z(t)$ is applied at the foundation. The TSPID is installed at the top floor, which is a common and effective location for controlling the fundamental mode in shear-type buildings. The particle mass $m_d = 0.42\text{kg}$ corresponds to approximately 5% of the total structural mass, a value consistent

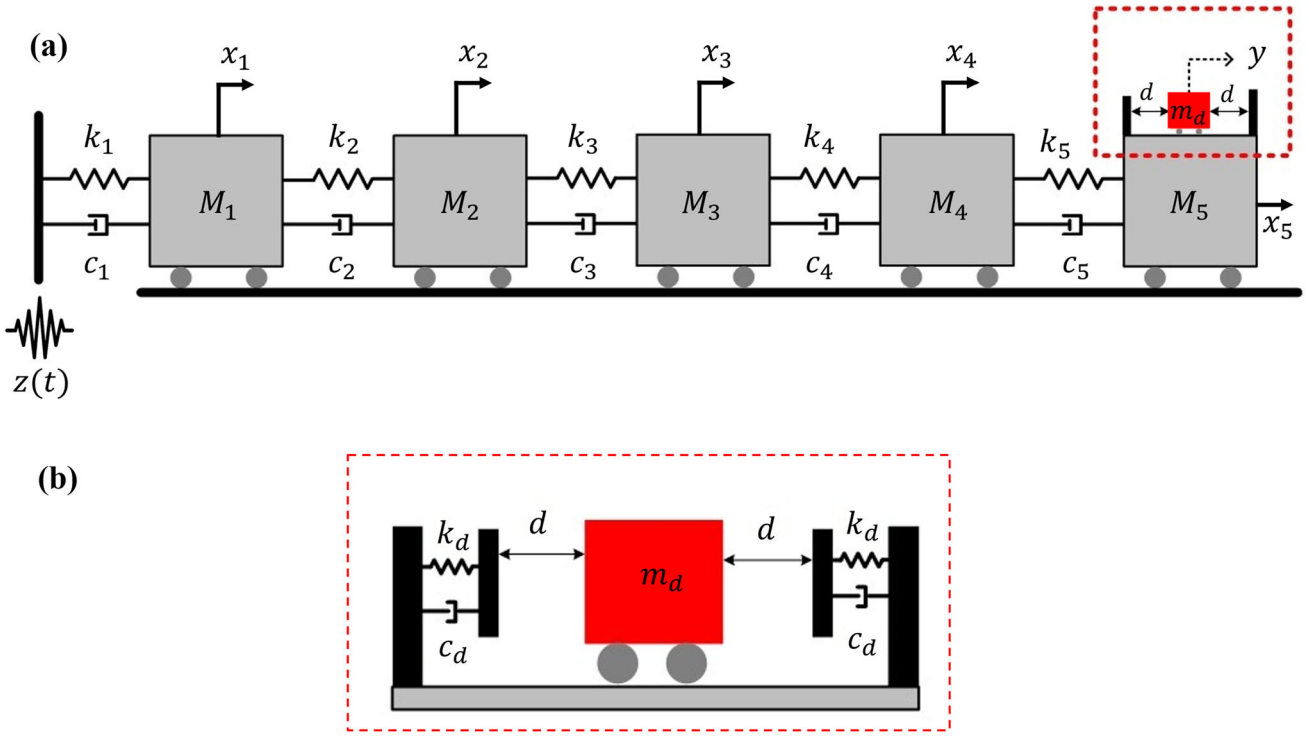


Fig. 1 **a** Equivalent mechanical model of 5-DOF structure **b** Mechanical model of TSPID

with the practical mass ratios reported in SPID studies and commonly adopted in particle damper applications to balance damping performance against added weight. Optimisation of the mass ratio is beyond the scope of this study; the focus here is on clearance as the primary geometric optimization parameter at fixed mass ratio. All system parameters are summarized in Table 1.

In the absence of the TSPID, the motion of each floor is governed by the standard second-order equations of motion for a shear building. When the TSPID is attached, the contact functions $G(\dot{x_5}, \dot{y})$ and $H(x_5, y)$ follow the classical piecewise-linear formulation originally developed by Masri for impact dampers. The coefficient of restitution e is incorporated into the model through the equivalent impact damping coefficient c_d. The impact stiffness k_d is set to $0.1k(\approx 337\mathrm{N/m})$ as a representative soft-impact value consistent with foam surfaces used in the experiments; parametric studies later confirm that this parameter has only minor influence compared with the clearance gap.

Table 1 System parameters

Parameters	Value
Mass of each floor M_{1-5}	1.71 kg
Stiffness of each floor k_{1-5}	3368.5
Mass of particle m_d	0.42 kg
Base excitation amplitude Z	1 mm

Friction in the linear guide of the TSPID is neglected in the numerical model because the low-friction bearings contribute negligible damping relative to the dominant impact dissipation, as evidenced by the close agreement between numerical and experimental results. Structural damping is assumed to be negligibly small, consistent with the lightly damped steel frame used in the experiments; this assumption is justified by the sharp resonance peaks observed in Fig. 7, which are characteristic of low-damping systems. The system is solved numerically using the fourth-order Runge–Kutta (RK4) method with a fixed time step of 0.001 s, selected after convergence analysis showed that smaller time steps yield negligible improvement in accuracy. The governing equations are expressed as follows:

$$M\ddot{x_1} + k_1(x_1 - z) + c_1(\dot{x_1} - \dot{z}) + k_2(x_1 - x_2) + c_2(\dot{x_1} - \dot{x_2}) = 0 \tag{1}$$

$$M\ddot{x_2} + k_2(x_2 - x_1) + c_2(\dot{x_2} - \dot{x_1}) + k_3(x_2 - x_3) + c_3(\dot{x_2} - \dot{x_3}) = 0 \tag{2}$$

$$M\ddot{x_3} + k_3(x_3 - x_2) + c_3(\dot{x_3} - \dot{x_2}) + k_4(x_3 - x_4) + c_4(\dot{x_3} - \dot{x_4}) = 0 \tag{3}$$

$$M\ddot{x_4} + k_4(x_4 - x_3) + c_4(\dot{x_4} - \dot{x_3}) + k_5(x_4 - x_5) + c_5(\dot{x_4} - \dot{x_5}) = 0 \quad (4)$$

$$M\ddot{x_5} + k_5(x_5 - x_4) + c_5(\dot{x_5} - \dot{x_4}) + k_dH(x_5, y) + c_dG(\dot{x_5}, \dot{y}) = 0 \quad (5)$$

The contact functions $H(x_5, y)$ and $G(\dot{x_5}, \dot{y})$ follows the established formulation for impact dampers [17, 19]. The function G models the spring force activation only when the particle–wall penetration exceeds the gap d. The function H similarly activates the damping force during contact. This piecewise-linear model is a standard representation for impact dynamics, balancing physical fidelity with computational efficiency for systems with clearances.

$$H(x_5, y) = (x_5 - y - d)U(x_5 - y - d) + (x_5 - y + d)U(-x_5 + y - d) \quad (6)$$

$$G(\dot{x_5}, \dot{y}) = (\dot{x_5} - \dot{y})U(x_5 - y - d) + (\dot{x_5} - \dot{y})U(-x_5 + y - d) \quad (7)$$

where d is the clearance between the particle and the walls of the TSPID container, also referred to as the "gap", and $U(x)$ is the unit-step (Heaviside) function, defined as:

$$U(x) = \begin{cases} 1, if x \geq 0 \\ 0, if x < 0 \end{cases}$$

This function is used to determine whether the particle is in contact with one side of the TSPID boundary. The output of $U(x)$ is either 0 or 1, depending on whether its argument is negative or non-negative. The contact force F_c exerted by the particle on the structure at any time step is calculated by combining the two contact functions with the corresponding stiffness and damping coefficients of the TSPID:

$$F_c = k_dH(x_5, y) + c_dG(\dot{x_5}, \dot{y}) \quad (8)$$

This contact force is applied only when the particle is in contact with the walls of the TSPID, i.e., when the relative displacement condition is satisfied. When the particle is not in contact, no force is transmitted to the primary structure, and the terms involving k_d and c_d have no effect. The equivalent viscous damping c_d is defined via an equivalent modal damping ratio ζ_{eq} (Eq. 9), which is directly related to the impact coefficient of restitution e through Eq. (10). This formulation links the energy loss during impacts to an equivalent linear damping representation.

$$c_d = 2\zeta_{eq}\sqrt{\frac{k_dm^2}{m + M}} \quad (9)$$

$$\zeta_{eq} = -\frac{\log(e)}{\sqrt{\pi^2 + \log(e)^2}} \quad (10)$$

For numerical simulations of the undamped 5-DOF system (i.e., without the TSPID), the parameters k_d and c_d can be set to zero. This allows for a baseline comparison between the damped and undamped systems to evaluate the effectiveness of the TSPID in suppressing vibrations.

The incorporation of the TSPID significantly increases the complexity of the system's dynamic behavior due to the nonlinear and discontinuous forces from impacts. The overall computational process is illustrated in the flowchart in Fig. 2. The procedure begins with the initialization of all system parameters, including mass, stiffness, damping coefficients, clearance distance d, and initial conditions for both the primary structure and the particle. The displacement of all degrees of freedom and the particle motion are then updated at each time step. If an impact is detected via the contact functions, the corresponding force from Eq. (8) is applied to the structure.

2.2 Experimental setup

A scaled five-story steel frame was designed and fabricated to replicate the 5-DOF system (Fig. 3). The TSPID is installed at the top floor, a common location for effective control of the fundamental mode in shear-type buildings. The particle mass is set at approximately 5% of the total structure mass to balance damping performance and added weight.

The structure consists of four vertical steel columns, each 765 mm tall with a 20 mm × 2 mm cross-section. Each floor is an aluminum block measuring 20 mm × 150 mm × 200 mm, providing nearly uniform mass distribution. The TSPID uses a linear guide rail that allows the particle to slide freely in one direction. Adjustable L-shaped stoppers at both ends define the clearance distance d.

The base is mounted on a shaking table driven by an electrodynamic shaker (Model: Econ VE−5150) capable of 500 N maximum force and 10 mm peak-to-peak displacement. The shaker supports sinusoidal, random, and sweep signals for versatile testing. Six non-contact laser displacement sensors (Model: Panasonic HG-C1200, ±80 mm range) measure the base and all five floor displacements. Non-contact sensing avoids interference with structural motion.

The experimental floor mass (including linear guide and stoppers) matches the value in Table 1 (1.71 kg). The inter-storey stiffness is calculated from beam theory as,

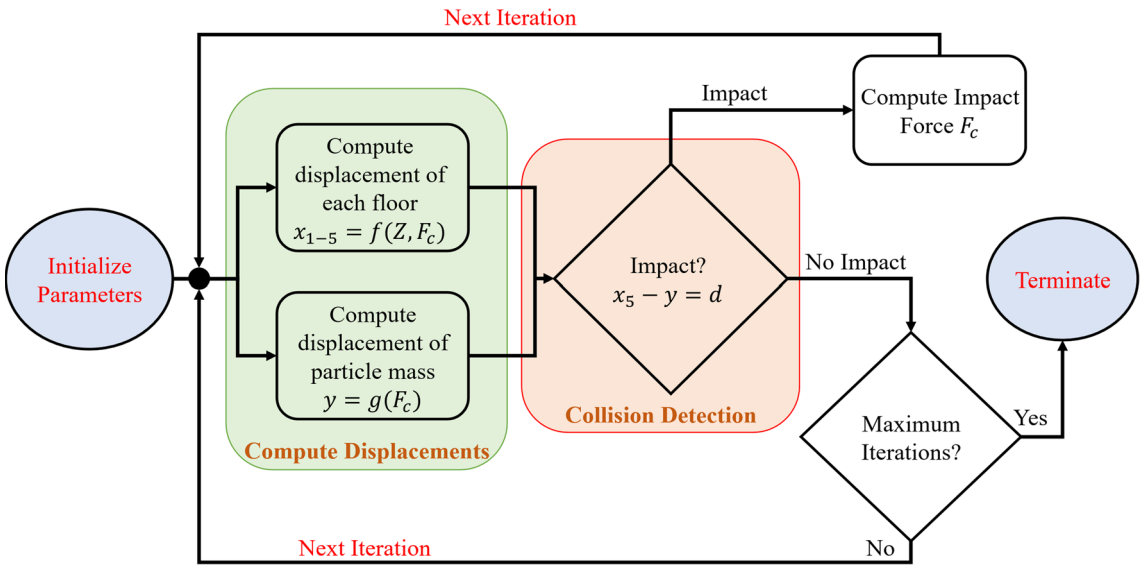


Fig. 2 Flow chart for the numerical computation process

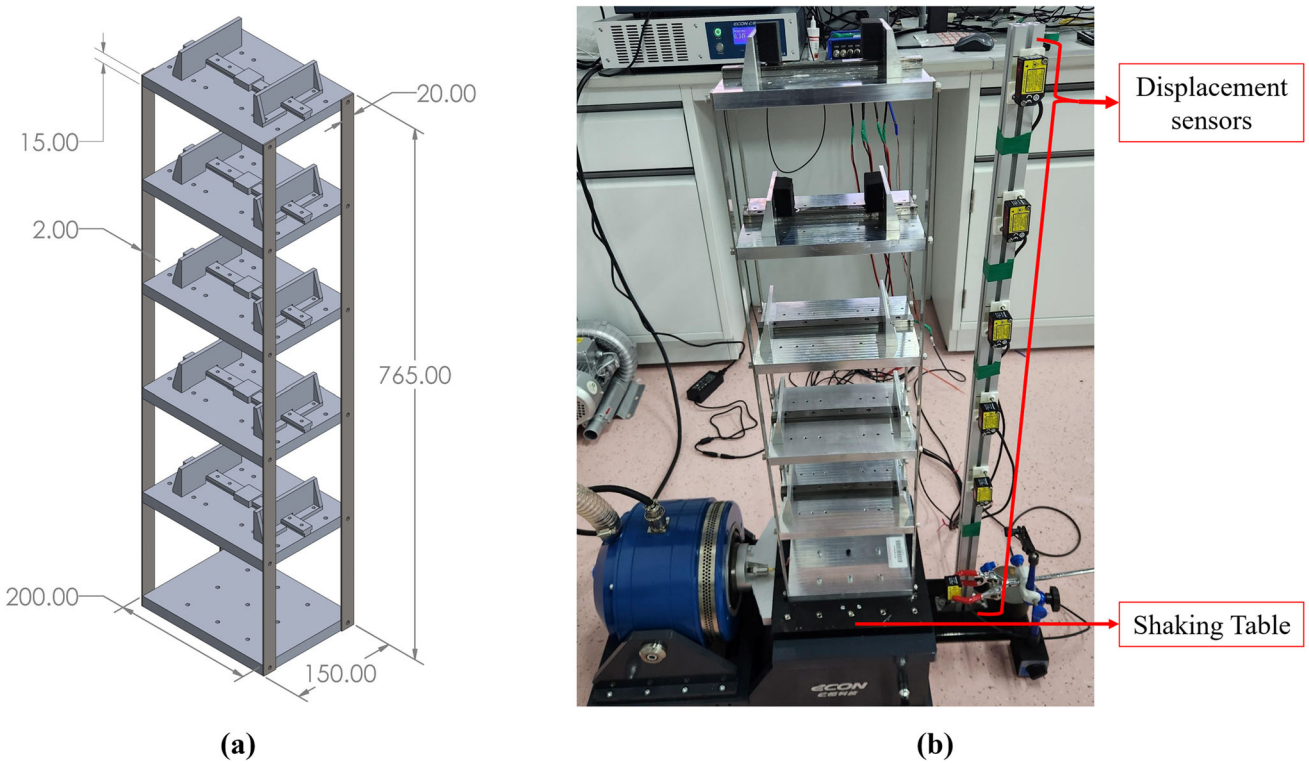


Fig. 3 **a** Design and dimensions in mm of the 5DOF structure; **b** Experimental rig and measurement system

$$k_i = 4\frac{12EI}{l^3} \tag{11}$$

$$I = \frac{bh^3}{12} \tag{12}$$

Here E is the Young's modulus of steel, l is the length of the column up to each mass, I is the second moment of area, b and h are the width and height of the column cross-section, and four columns act in parallel. The total column height is divided into five equal story heights for stiffness calculation.

Due to the highly nonlinear impact mechanism of the TSPID, a conventional continuous sine-sweep test is unsuitable. The damper requires sufficient oscillation amplitude and multiple impact cycles to reach steady-state energy dissipation at each frequency. A fast sweep may miss impacts, while a sufficiently slow sweep would result in impractically long test durations. Therefore, a frequency-by-frequency approach was adopted. Natural frequencies were first identified with a preliminary test where discrete sinusoidal excitations were applied for 20s at selected frequencies near each resonance to ensure steady-state conditions. Harmonic excitation at each modal resonance frequency was selected as it provides the most direct assessment of mode-selective analysis. It should be noted that a conventional sweep test was performed initially to only identify the natural frequencies of the bare structure. However, the present study focuses on the first two natural frequencies, where mode-selective behaviour is most clearly demonstrated. All tests used a base excitation amplitude of 1 mm.

2.3 TSPID prototype

Fig. 4 shows the prototype, which consists of two adjustable stoppers, a moving aluminum-plate particle mass, and an interchangeable impact surface.

Two commonly available foam materials were used as the impact surface: polyurethane (PU) foam with a measured coefficient of restitution $e = 0.38$ and polyethylene (PE) foam with $e = 0.72$. These values were obtained from repeated drop tests and represent the range of soft-to-moderately stiff impact behaviour [62]. The clearance gap was adjusted by repositioning the stoppers to achieve the normalized values determined numerically for each mode. The input excitation amplitude was fixed at 1 mm to maintain the target normalized clearance $D = \frac{d}{Z}$.

3 Numerical parametric design study and optimization parameters

The TSPID design parameters were examined through a systematic numerical parametric study to identify the optimal configuration for maximum vibration attenuation around a single targeted resonance frequency. For each combination of parameters, the system was simulated in the time domain using the RK4 integrator. The modal $H_{i,\infty}$ norm around the resonance frequency f_i was then extracted as the objective function to be minimized:

$$H_{i,\infty} = max\left|\frac{X_{top(f)}}{Z(f)}\right| \text{for} f \in [f_i - 1Hz, f_i + 1Hz],$$

where i represent the respective mode (i.e. $i = 1, 2$). This formulation directly targets the worst-case peak response, which is the primary design goal for vibration suppression. Only the top-floor response was used for optimization to reduce computational cost while focusing on the most critical location.

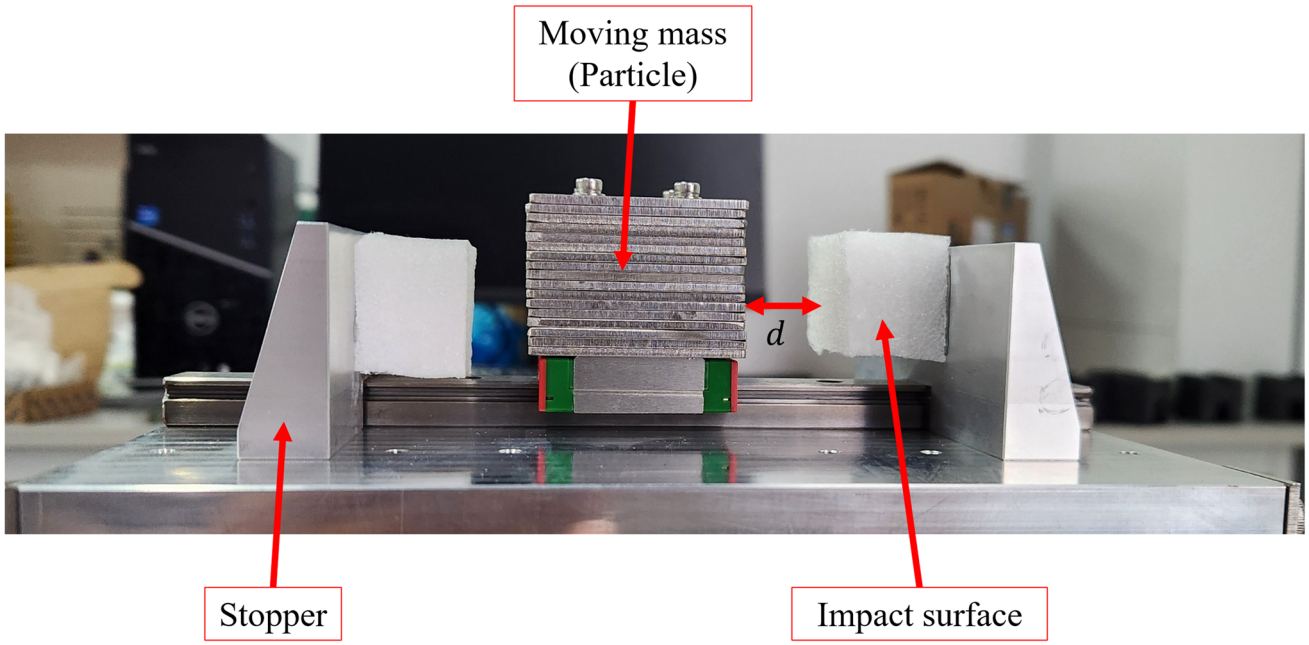


Fig. 4 Prototype of TSPID where stoppers, moving mass (particle) and impact surface is shown

The first two natural frequencies of the undamped structure are approximately 6.4 Hz and 18.7 Hz. Simulations were performed over the ranges 5.5–7.5 Hz for mode 1 and 18–20 Hz for mode 2 using a frequency step of 0.05 Hz. At each discrete frequency, a 20 s time-domain simulation was conducted, and the maximum displacement was extracted from the final 10 s of the steady-state response to eliminate transient effects. This process generated localized frequency response curves for every parameter combination, from which the modal $H_{i,\infty}$ norm was obtained.

The resulting contour plots of the modal $H_{i,\infty}$ norm versus normalized clearance $D = \frac{d}{Z}$ and coefficient of restitution e (with k_d initially fixed at $0.1k$) are presented in Fig. 5. The contour plots emphasize that the normalized clearance gap D exerts the strongest influence on TSPID performance. For the first mode (Fig. 5a), the lowest $H_{1,\infty}$ norm values occur in the range $D \approx 6 - 11$. For the second mode (Fig. 5b), optimal performance shifts to a distinctly smaller range $D \approx 1 - 2$. Within the studied range, the coefficient of restitution e produces only secondary effects.

A reasonable value of e in the range 0.2–0.6 was therefore selected for subsequent simulations. This choice follows from the trade-off in impact-damper literature: higher restitution coefficients produce stronger rebound velocities, which increase both the peak impact force transmitted to the structure and the audible noise generated during collisions [34]. Conversely, very low values of e can lead to excessive energy dissipation per impact but may also prolong contact duration and reduce overall effectiveness at higher frequencies. Subsequent simulations held e constant at 0.4 value and explored the interaction between D and normalized impact stiffness $\frac{k_d}{k}$. The corresponding contour plots appear in Fig. 6.

These results indicate that clearance remains the controlling parameter across both modes, while the influence of impact stiffness stays limited except at very small D values where tuned-mass-damper behaviour emerges. The observed difference in optimal D between modes is associated with the different oscillation periods and response amplitudes of the two modes.

The optimal normalized clearance $D = \frac{d}{z}$ is not merely a convenient non-dimensional term but a physically meaningful design parameter encoding the amplitude-clearance interaction that governs impact effectiveness. This can be understood through a limiting argument: an undersized gap relative to excitation amplitude drives chaotic, asynchronous particle motion that loses phase coherence with the structure, while an oversized gap results in infrequent or no impacts. As shown by Duncan et al. [63], damping effectiveness approaches the detuned case at both amplitude extremes, with peak performance occurring at intermediate amplitudes where the particle just reaches the boundary; for sufficiently large clearance ratios, further amplitude increases have limited influence on damping. The optimal D therefore represents the amplitude-clearance condition at which the particle achieves consistent, phase-coherent engagement with the structural motion. Consequently, for a given optimal D, the physical gap d must scale proportionally with excitation amplitude to preserve this condition, if the operating amplitude changes, d should be rescaled accordingly

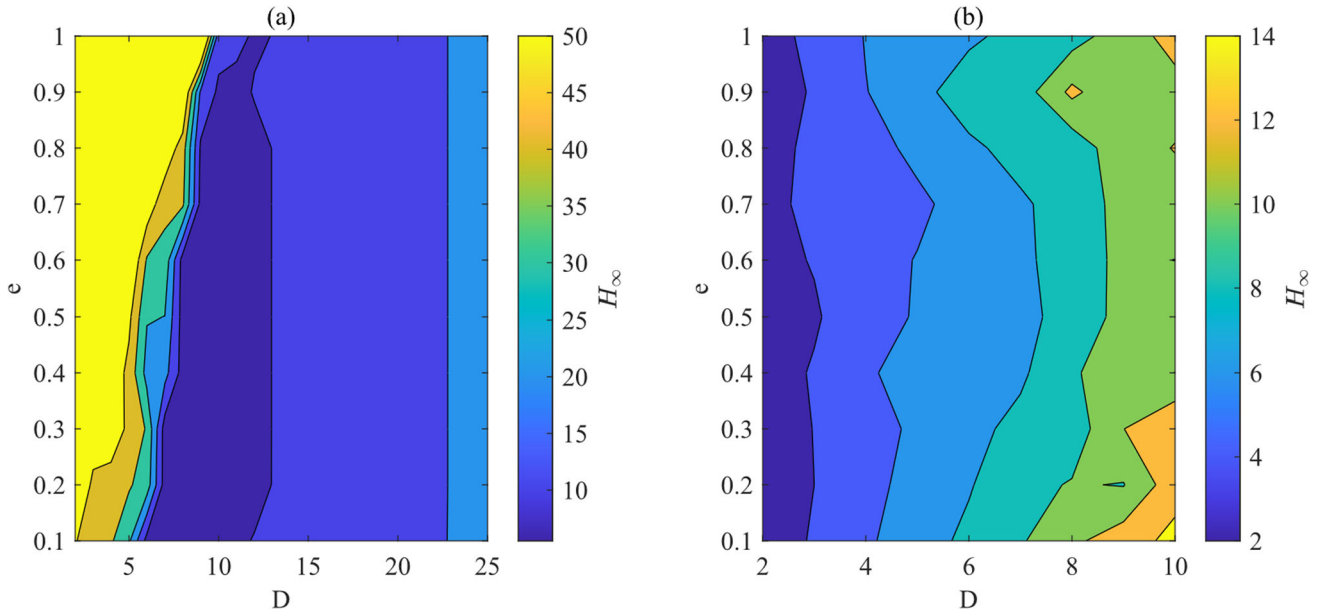


Fig. 5 Modal $H_{i,\infty}$ norm at various combinations of e and D while $k_d = 0.1k$ for **a** $H_{1,\infty}$ re vibration mode 1 $[5.5 - 7.5\text{Hz}]$; **b** $H_{2,\infty}$ re vibration mode 2 $[18 - 20\text{Hz}]$

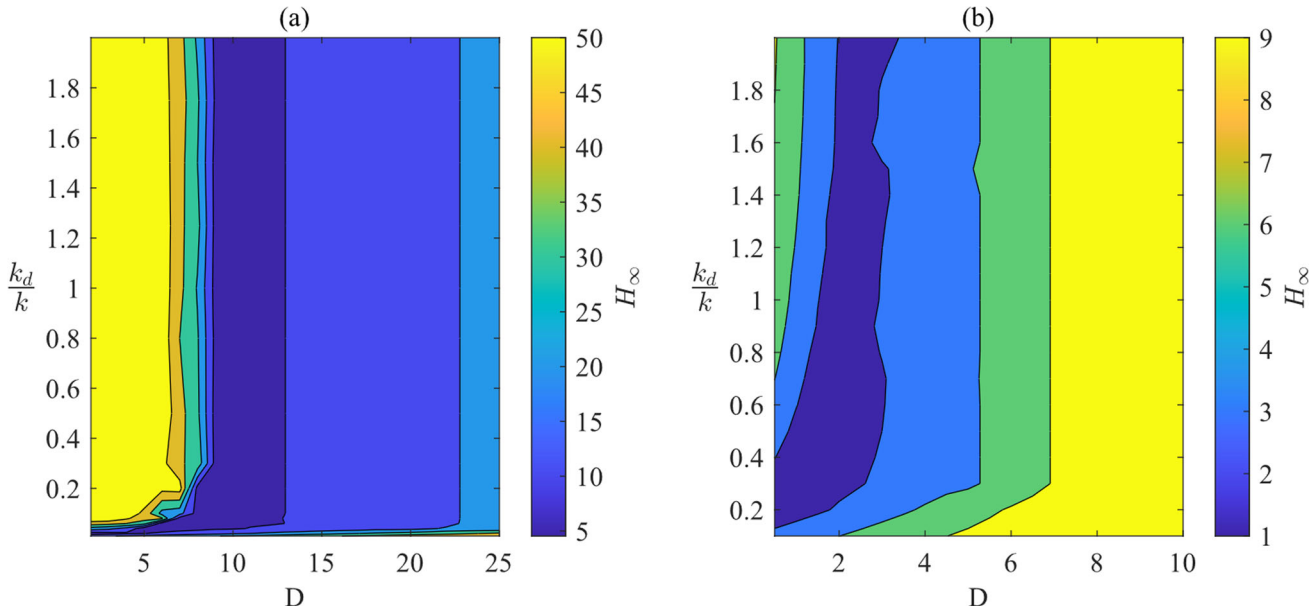


Fig. 6 Modal $H_{i,\infty}$ norm at various combinations of D and k_d, while $e = 0.4$ for **a** $H_{1,\infty}$ re vibration mode 1 $[5.5 - 7.5\text{Hz}]$ **b** $H_{2,\infty}$ re vibration mode 2 $[18 - 20\text{Hz}]$

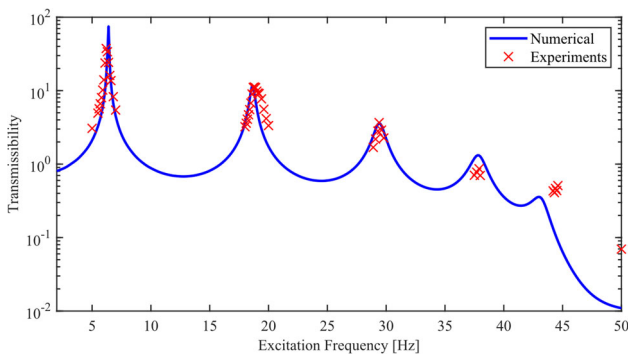


Fig. 7 Comparison of simulated and experimental base-floor to top-floor transmissibility

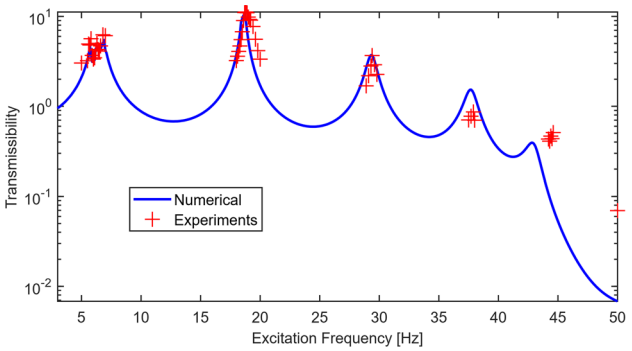


Fig. 8 Comparison of simulated and experimental base-floor to top-floor transmissibility with TSPID using PU foam parameters. $k_d = 0.1k$. $D = 12$

rather than redesigning the device entirely. This is consistent with the observation that different modes exhibit different optimal clearances. This behaviour supports a straightforward geometric optimization strategy that reduces reliance on precise material characterization.

Notably, D emerges as the primary geometric parameter governing the impact behaviour and energy dissipation characteristics of the TSPID. Unlike TMDs, which depend on accurate tuning of stiffness and damping to match target frequencies, the TSPID achieves targeted attenuation through adjustment of D alone, thereby reducing sensitivity to parameter uncertainties and detuning effects.

4 Results and discussion

This section compares numerical simulations and experimental results for the 5-DOF structure with and without the TSPID.

4.1 Model validation

First, the model validation results are presented in this section. Figure 7 shows the comparison of simulated and experimental base to top-floor transmissibility for the bare structure across all natural frequencies, confirming the accuracy of the numerical model prior to damper optimization.

To validate the coupled model prior to the parametric study, numerical predictions are compared against

experimental measurements with the TSPID with $D = 12$. Figure 8 presents the transmissibility of the structure with TSPID, comparing numerical and experimental results. The close agreement between the two confirms that the contact model parameters k_d and c_d are appropriately defined and that the nonlinear coupled model reliably captures the structural response in the presence of impacts.

4.2 TSPID optimization and modal $H_{i,\infty}$ norm reduction across storey

This section presents the effect of TSPID on the maximum vibration amplitude (modal $H_{i,\infty}$ norm) at each floor of the structure. The results from both experimental tests and numerical simulations are compared to validate the numerical model and demonstrate its effectiveness in identifying optimal design parameters. With the optimal normalized clearance values identified in the parametric study, a physical TSPID prototype was designed and installed on the top floor of the structure.

First, the TSPID was optimized for the first mode using the optimal normalized clearance $D \approx 8$. The measured resonance frequencies were 5.9 Hz for mode 1 and 18.6 Hz for mode 2. The modal $H_{i,\infty}$ norm at each floor was recorded both with and without the damper. The results are presented in Fig. 9.

As shown in Fig. 9a, when the TSPID is optimized for mode 1 the modal $H_{1,\infty}$ norm is reduced by an average of 86% across all floors for both foam materials. Excellent agreement is observed between numerical simulations and experimental measurements. In contrast, Fig. 9b demonstrates that the same configuration produces negligible reduction at the second mode ($H_{2,\infty}$). This frequency-selective behaviour is expected because the larger clearance optimised for the lower-frequency mode does not generate sufficient impacts within the shorter oscillation period of the higher mode.

The TSPID was then optimized for the second mode by reducing the normalized clearance to $D \approx 2$, again using both PU and PE foams. The corresponding modal $H_{i,\infty}$ norm results are shown in Fig. 10. Figure 10a confirms that the second-mode tuning has minimal influence on the first mode. However, Fig. 10b shows a clear reduction in modal $H_{2,\infty}$ norm, reaching an average of 66% with PE foam and 58% with PU foam. The slightly superior performance of PE foam at the higher frequency is consistent with the need for a marginally higher impact stiffness to ensure timely momentum exchange during the shorter vibration cycles. Literature on impact dampers indicates that at elevated frequencies the contact duration becomes a limiting factor, and a stiffer interface helps maintain effective energy transfer without excessive rebound [34, 64].

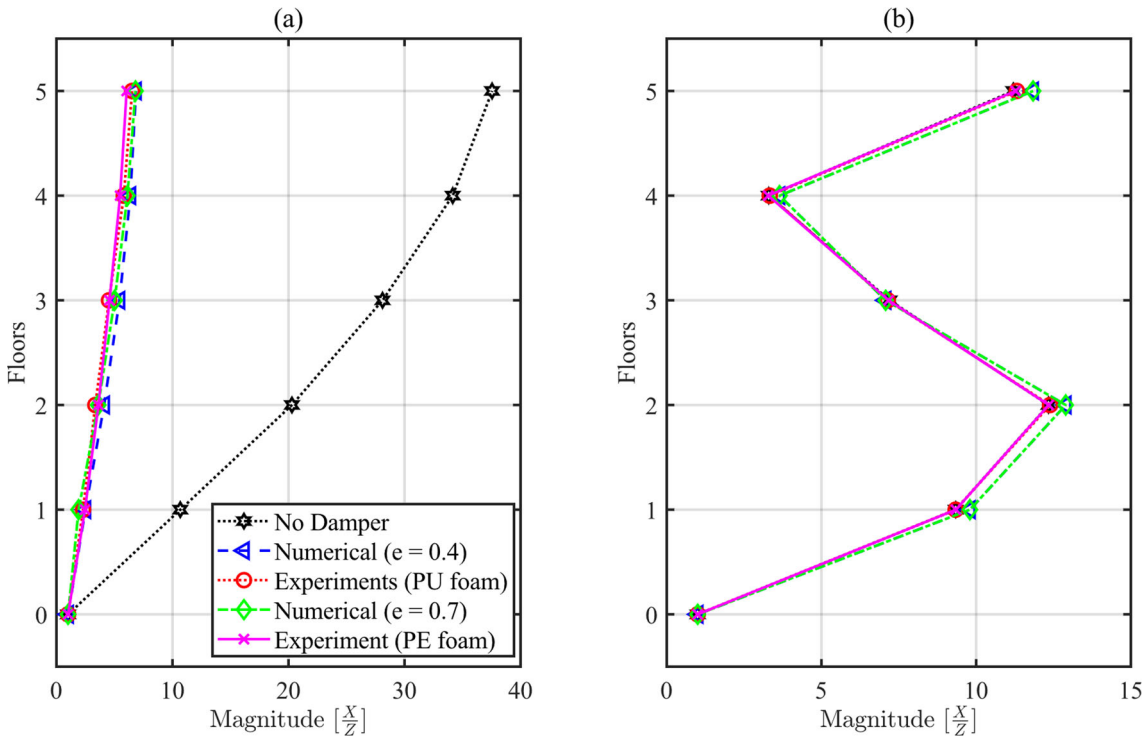


Fig. 9 Modal $H_{i,\infty}$ with TSPID optimized for mode 1, $D \approx 8$ **a** Mode 1 [5.9Hz] **b** Mode 2 [18.6Hz]

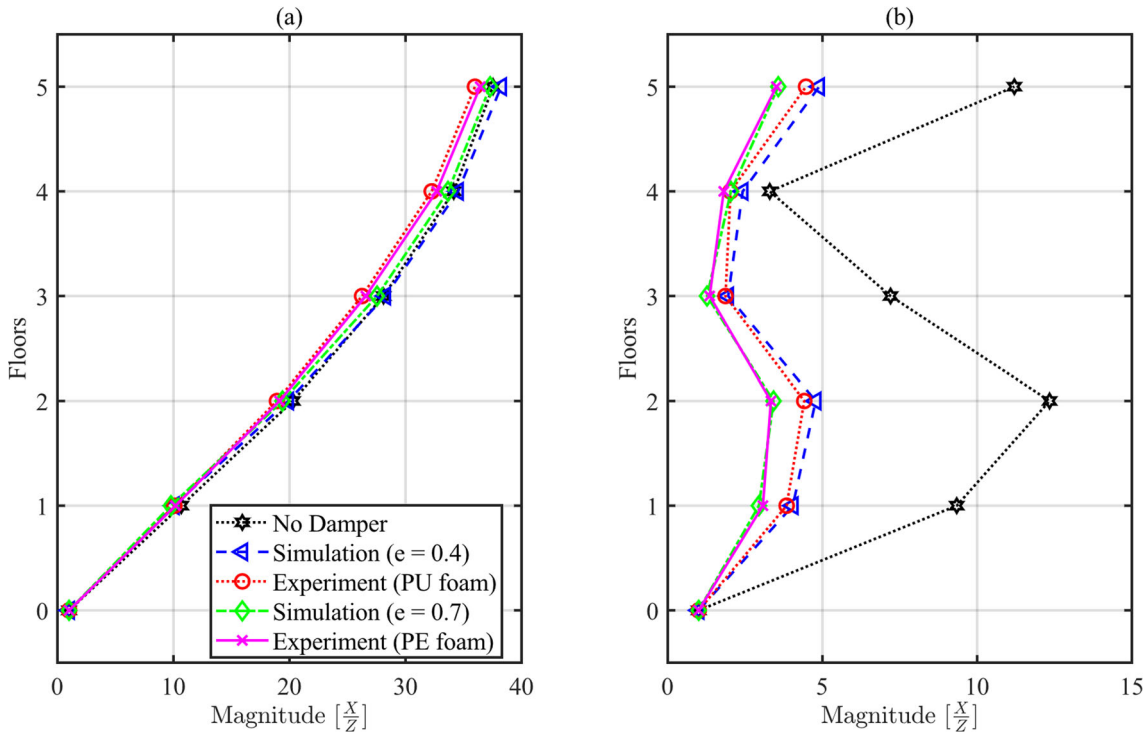


Fig. 10 Modal $H_{i,\infty}$ with TSPID optimized for mode 2, $D \approx 2$. **a** Mode 1 [6.05Hz] **b** Mode 2 [18.45Hz]

These experiments demonstrate that the TSPID can achieve substantial, mode-specific suppression of the modal $H_{i,\infty}$ norm using only a single geometric parameter. The clear trade-off between the two modes underscores the importance of clearance optimization and confirms that the damper's performance is governed primarily by clearance rather than exact material properties.

4.3 TSPID optimization and Vibration Energy reduction across storey

Vibration energy distribution across the floors was analyzed using experimental time-history data. Measuring vibration energy is particularly important because it quantifies the total dynamic energy present in the structure, providing a direct indicator of the damper's ability to dissipate kinetic energy through impacts rather than merely reducing peak displacement at resonance. This metric complements the modal $H_{i,\infty}$ norm by revealing how effectively the TSPID redistributes and dissipates energy across the entire system, which is critical for assessing overall vibration control performance under resonant excitation. The energy of each floor i is calculated as

$$E_i(t) = \frac{1}{2} m_i \dot{x}_i^2(t) \tag{13}$$

The normalized vibration energy at each floor is calculated as the root-mean-square (rms) kinetic energy of floor i computed from the undamped response at the same excitation frequency. Here E_i, m_i, $\dot{x}_i$ represent the energy, mass, and velocity of each floor, where $i = 1,2,3,4,5$. The velocity is derived from the discrete displacement data using central difference method [65, 66] as shown in Eq. 14,

$$\dot{x}_i(t) = \frac{x_i(t+1) - x_i(t-1)}{2\Delta t} \tag{14}$$

This method reduces noise sensitivity compared to forward differences [67, 68]. The resulting energy values were then low-pass filtered to minimize any residual numerical noise.

When the TSPID is optimized for the first mode with normalized clearance $D \approx 8$, the normalized vibration energy is reduced by an average of 95% across all floors for both PU and PE foams. The results for mode 1 and mode 2 with this tuning are shown in Fig. 11. The results in Fig. 11a demonstrate that the TSPID achieves a 95% reduction in normalized vibration energy at the first mode. The performance obtained with PU foam ($e = 0.38$) and PE foam ($e = 0.72$) differs by less than 5% across all floors. This near-identical outcome with two foams of distinctly different restitution coefficients confirms that the clearance gap is the dominant design parameter and that

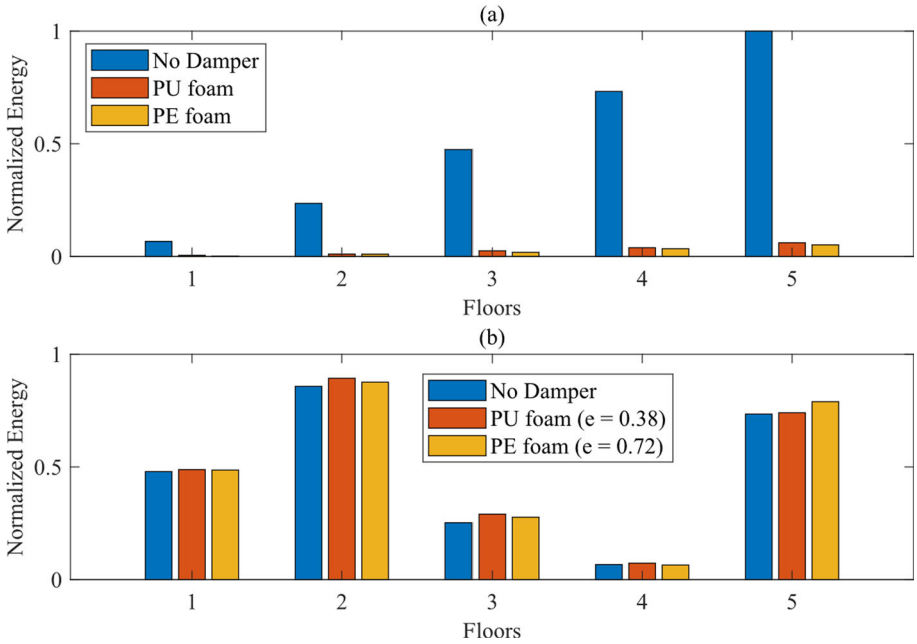


Fig. 11 Normalized vibration energy with TSPID optimized for mode 1, $D \approx 8$ **a** Mode 1 [5.9Hz] **b** Mode 2 [18.6Hz]

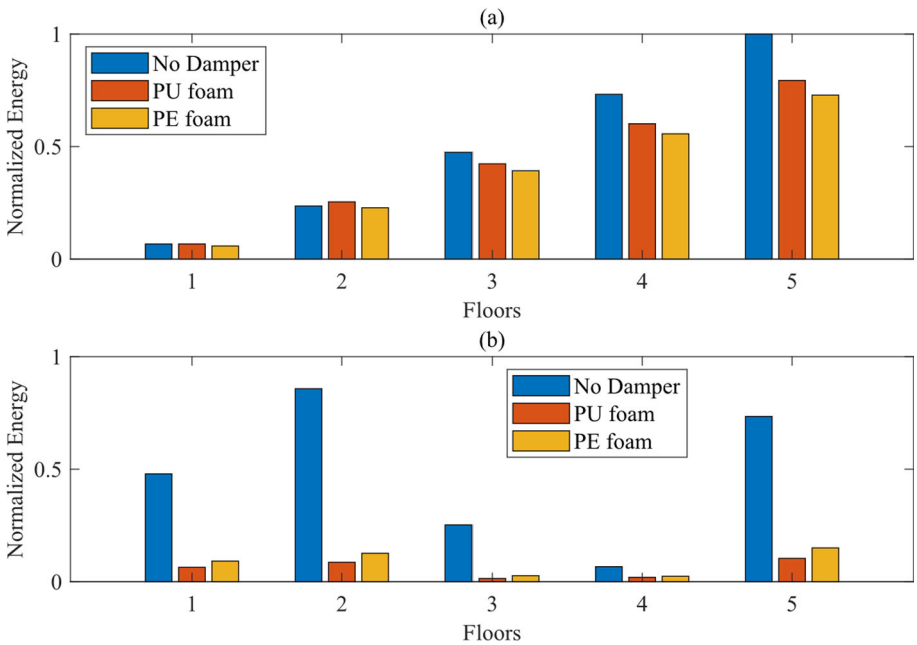


Fig. 12 Normalized vibration energy with TSPID optimized for mode 2, $D \approx 2$ **a** Mode 1 [6.05Hz] **b** Mode 2 [18.45Hz]

the TSPID dissipates energy primarily through impact dynamics. This robustness is consistent with the relatively flat modal $H_{i,\infty}$ contour region observed in Fig. 6 for moderate restitution values; performance at extreme restitution values (e near 0 or near 1) was not tested and may differ. It highlights the damper's effectiveness in converting oscillatory kinetic energy into heat and plastic deformation during repeated particle–wall collisions. In contrast, the same tuning produces negligible energy reduction at the second mode (Fig. 11b), again underscoring the frequency-selective nature of the device.

When the TSPID is instead optimized for the second mode with $D \approx 2$, the average reduction in vibration energy reaches 85% at the target frequency (Fig. 12b), while the effect on the first mode remains small (Fig. 12a).

4.4 Inter-storey drift

Inter-storey drift (ISD), defined as the rms relative horizontal displacement between consecutive floors, serves as a critical serviceability metric in structural engineering. Excessive ISD can cause non-structural damage such as

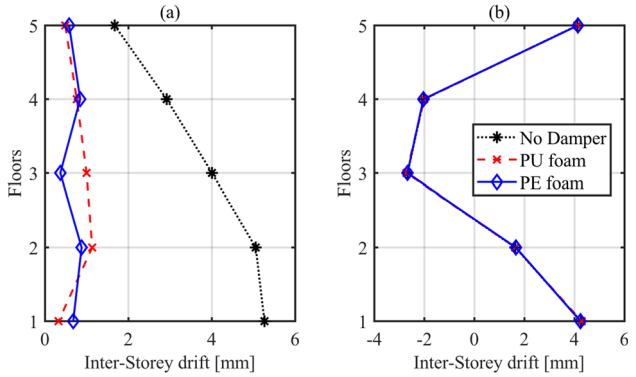


Fig. 13 Inter-storey drift with TSPID optimized for mode 1, $D \approx 8$ **a** Mode 1 [5.9Hz] **b** Mode 2 [18.6Hz]

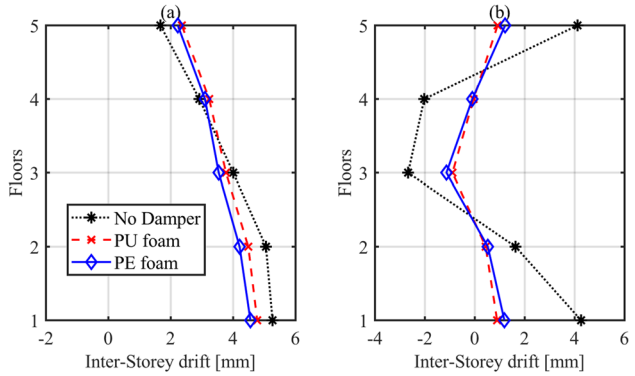


Fig. 14 Inter-storey drift with TSPID optimized for mode 2, $D \approx 2$ **a** Mode 1 [6.05Hz] **b** Mode 2 [18.45Hz]

cracking of partitions and cladding failure, and in severe cases may compromise overall structural integrity. Therefore, effective control of ISD is essential for both safety and serviceability under dynamic loading. For reference, serviceability drift limits in design codes are typically in the range of 0.5% of storey height for seismic loading [69, 70].The present scaled model is not designed to meet full-scale code thresholds directly; however, the magnitude of undamped ISD observed here, and the substantial reductions achieved by the TSPID, are consistent with the order-of-magnitude improvements needed in resonance-dominated structural scenarios.

The ISD was computed directly from the steady-state displacement time histories recorded during the frequency-by-frequency tests. Figure 13 presents the ISD values when the TSPID is optimized for the first mode with normalized clearance $D \approx 8$. When optimized for mode 1, the TSPID reduces ISD by an average of 93% across all floors at the target frequency (Fig. 13a), while producing negligible reduction at the second mode (Fig. 13b). The results are nearly identical for both PU and PE foam configurations.

When the TSPID is optimized for the second mode with $D \approx 2$, the ISD reduction at the target frequency reaches an average of 79% (Fig. 14b), while the influence on the first mode remains small (Fig. 14a).

Table 2 quantifies the percentage improvement in ISD at each floor for both tuning cases and both foam materials. The largest reductions occur near the base for mode 1 and in the middle-to-upper floors for mode 2, consistent with the respective mode shapes. The small difference observed between PU and PE foams at mode 2 is attributable to the relatively higher impact stiffness of PE foam, which becomes more relevant at elevated frequencies where the available contact time is limited. Previous studies on impact dampers have noted that a stiffer interface can improve momentum transfer efficiency under shorter oscillation periods [34, 71, 72].

Table 2 Percentage improvement in ISD at each floor for the first two modes with respectively tuned TSPID

	Mode 1		Mode 2	
	$D \approx 8$		$D \approx 2$	
Floor	PU	PE	PU	PE
1	93.86	87.16	79.02	72.17
2	77.62	82.65	73.27	68.00
3	75.12	90.84	66.52	57.47
4	73.94	71.12	97.49	95.04
5	70.99	65.40	77.82	70.50

These results show that the TSPID can simultaneously achieve high reductions in inter-storey drift along with the previously discussed improvements in modal $H_{i,\infty}$ norm and vibration energy. The ability to target specific modes through a single adjustable clearance makes the TSPID a versatile and practical solution for controlling both peak response and serviceability metrics in MDOF structures.

4.5 Time-history analysis

Time-history displacement responses provide direct visualization of the TSPID's effect on the structural motion under resonant excitation.

Only experimental data are shown in this section to allow clear observation of the actual measured behaviour and to avoid overcrowding the plots with overlapping numerical curves. When optimized for the first mode with $D \approx 8$, the TSPID produces a substantial reduction in displacement amplitude, the corresponding time histories are shown in Fig. 15. Both PU and PE foam configurations yield similar amplitude reductions and display a clear phase lag compared with the undamped response. This phase lag arises primarily from the additional energy dissipation caused by the repeated particle impacts. The same

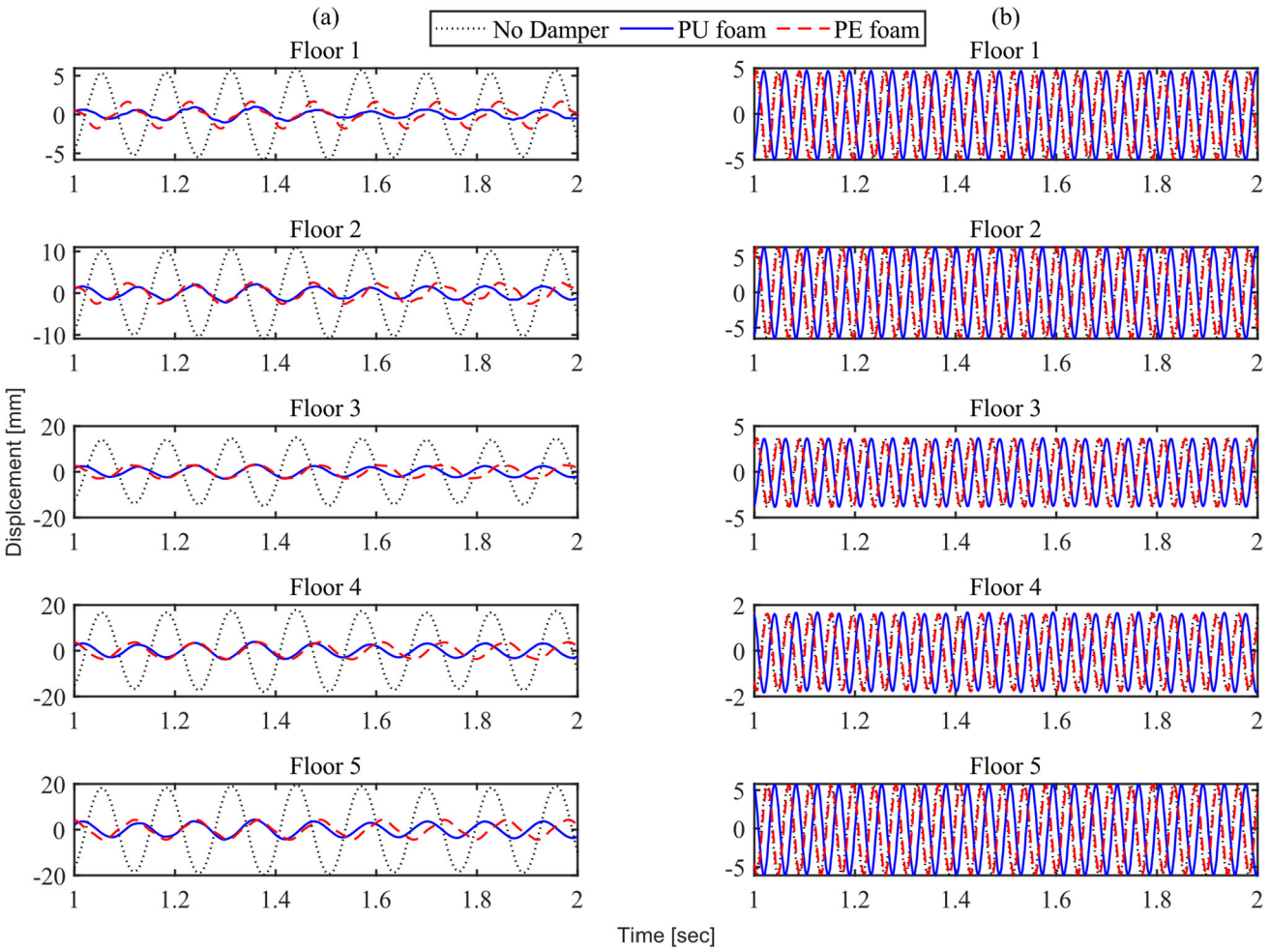


Fig. 15 Time-history displacement of each floor of the structure with TSPID optimized for mode 1, $D \approx 8$. **a** Mode 1 [5.9Hz] **b** Mode 2 [18.6Hz]

tuning configuration shows almost no reduction when the structure is excited at the second mode frequency of 18.6 Hz (Fig. 15b).

When the TSPID is optimized for the second mode with D $\approx$ 2, the time histories reveal the frequency-selective nature of the damper. At the first mode frequency (6.05 Hz), the amplitude reduction remains minimal (Fig. 16a). At the second mode frequency (18.45 Hz), however, significant suppression occurs across all floors (Fig. 16b). The response at the second mode exhibits more pronounced nonlinear characteristics, with distorted waveforms resulting from the intermittent nature of the impact events. This behaviour is examined in detail in the Impact Analysis section. A consistent phase lag between the damped and undamped cases is again observed. This lag is mainly attributed to the energy dissipation mechanism rather than the small added mass of the TSPID.

The time-history results are consistent with the frequency-domain and energy analyses presented earlier. They confirm that the TSPID can deliver strong vibration attenuation at a targeted mode while leaving other modes largely unaffected when tuned appropriately. This selective behaviour demonstrates the potential of the proposed damper for precise modal control in MDOF structures. It should be noted that the present study evaluates performance only at the first two resonance frequencies; the response at higher modes and under off-resonance or broadband excitation was not assessed and represents a limitation of the current experimental scope.

4.6 Impact analysis

To further characterize the impact behaviour associated with mode-selective suppression, three clearance values were selected for impact characterization. $D = 8$ and $D = 2$ represent the numerically identified and experimentally validated optimal clearances for the first and second modes respectively, as established in the preceding parametric study. These two values are therefore of primary interest as they represent the conditions corresponding to the

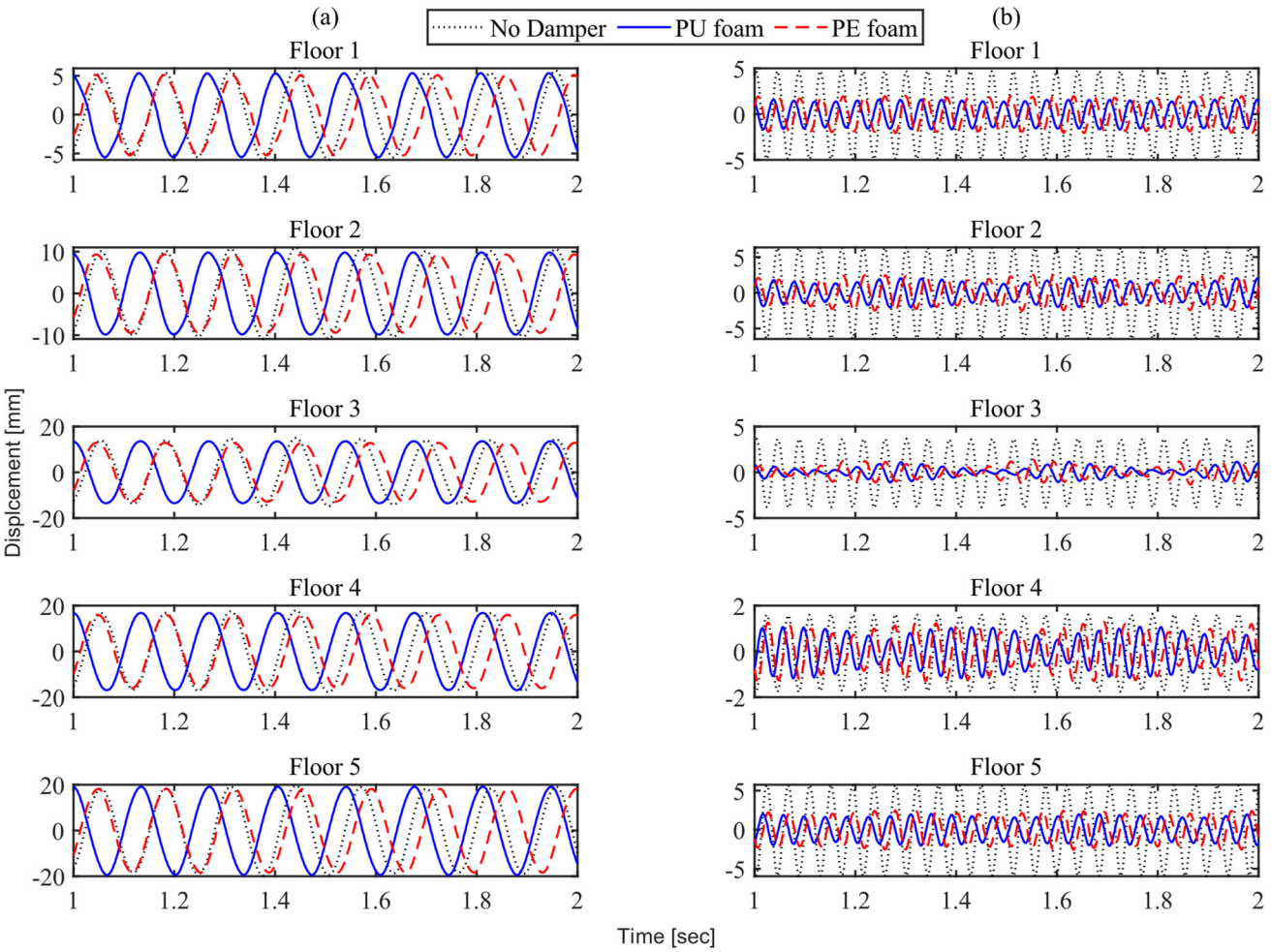


Fig. 16 Time-history displacement of each floor of the structure with TSPID optimized for mode 2, $D \approx 2$. **a** Mode 1 [6.05Hz] **b** Mode 2 [18.45Hz]

optimized clearance for each target mode. A third value, $D = 14$, was selected as a deliberately off-optimal case, lying well outside the effective clearance range for either mode, to provide a reference against which the impact behaviour of the optimal configurations can be contrasted. By examining all three cases together, the analysis reveals not only what makes the optimal clearances effective, but also why clearances outside the optimal range fail to achieve meaningful suppression at either modal frequency. Impact events were identified numerically as the onset of non-zero contact force between the particle and the cavity wall, with a minimum temporal separation enforced between consecutively counted events to avoid numerical double-counting of a single physical collision. The mean relative velocity between the particle and the host floor at each impact onset was recorded as a proxy for momentum transfer per impact.

Fig. 17 presents the impacts per cycle and mean impact velocity across the excitation frequency range for $D = 2$, $D = 8$, and $D = 14$. At the first modal frequency, $D = 2$ reaches approximately 3 impacts per cycle, indicating that the small clearance is repeatedly and easily crossed by the large Mode 1 displacement. However, the corresponding mean impact velocity for $D = 2$ at Mode 1 is comparatively low, revealing that although contact is frequent, each collision carries limited momentum and contributes little to energy dissipation. This is the hallmark of an ineffective high-frequency rattling regime. In contrast, $D = 8$ at Mode 1 achieves close to 2 impacts per cycle with a notably higher mean impact velocity, consistent with the symmetric double-impact pattern of efficient resonance capture where the particle builds sufficient momentum across the full clearance before returning to strike the opposite wall. At the second modal frequency, the roles reverse clearly: $D = 2$ produces approximately 2 regular impacts per cycle with peak mean impact velocity, confirming effective resonance capture at Mode 2. Meanwhile $D = 8$ at Mode 2 shows significantly reduced impact frequency, as the larger

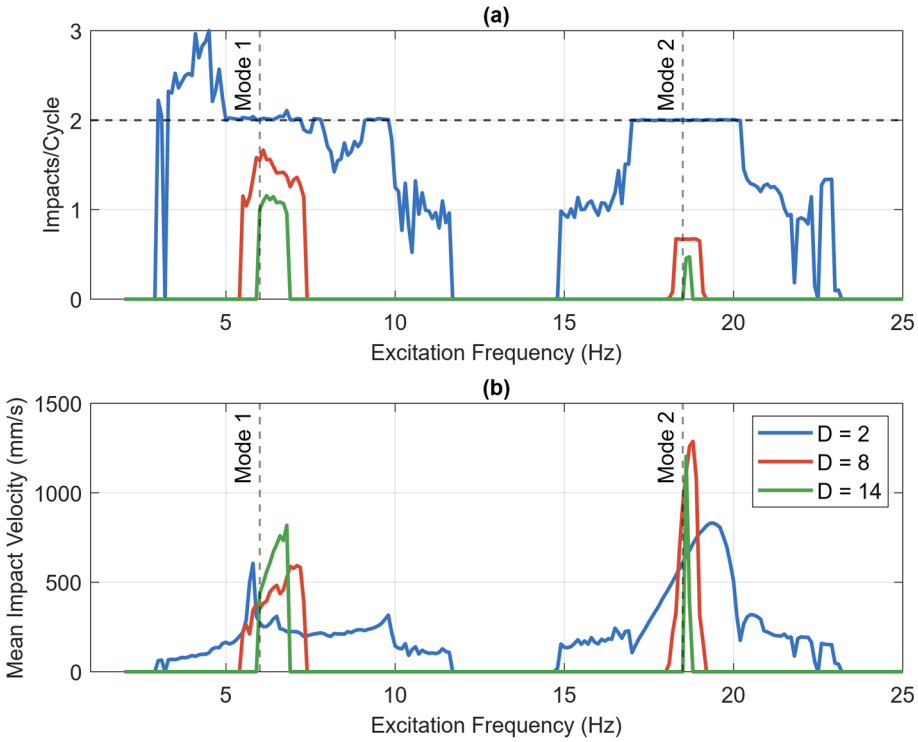


Fig. 17 **a** Impacts per cycle for different values of D for first two modes. **b** Mean Impact velocity for different values of D

clearance is rarely fully traversed at the smaller Mode 2 response amplitudes. The off-optimal case $D = 14$ produces fewer than 2 impacts per cycle at both modal frequencies. However, the larger clearance allows the particle to travel further between walls, resulting in comparatively higher mean impact velocity per collision. Despite this, the significantly reduced contact frequency means that the total momentum exchange per cycle remains insufficient for effective vibration suppression.

This illustrates that neither impact frequency nor impact velocity alone determines damping effectiveness, both must be simultaneously adequate at the target modal frequency. These results demonstrate that effective vibration suppression requires the simultaneous satisfaction of two conditions: approximately 2 regular impacts per cycle and sufficiently high mean impact velocity at the target modal frequency. The clearance D governs both conditions together by controlling whether the particle can complete a full traversal and return with meaningful momentum within one structural oscillation period. These observations indicate that effective impact-mediated energy transfer is associated with the simultaneous occurrence of approximately two impacts per cycle and sufficiently high impact velocity at the target modal frequency.

5 Conclusion

This study has developed and experimentally validated a Tuned Single-Particle Impact Damper (TSPID) for targeted modal vibration suppression in multi-degree-of-freedom structures. Systematic numerical parametric studies combined with frequency-by-frequency experiments on a scaled five-story shear-type building identified the clearance gap D as the dominant geometric parameter governing the optimized suppression performance. When optimized for the first mode ($D \approx 8$), the TSPID achieved average reductions of 86% in modal $H_{1,\infty}$ norm, 95% in vibration energy, and 93% in inter-storey drift across all floors. When optimized for the second mode ($D \approx 2$), the corresponding reductions were 66% in modal $H_{2,\infty}$ norm, 85% in vibration energy, and 79% in inter-storey drift. These results were obtained using only a single geometric adjustment on the clearance gap and remained consistent across two foams with distinctly different restitution coefficients ($e = 0.38$ for PU and $e = 0.72$ for PE), with differences below 5% in most metrics.

The observed mode-selective behaviour is associated with the dependence of the optimized clearance on the dynamic characteristics of the target mode. The normalized clearance was found to be a physically meaningful design parameter, encoding the amplitude-clearance interaction that governs impact effectiveness: different modes exhibit different response amplitudes, resulting in different optimized physical clearances. Numerical impact sequencing

analysis further shows that at each optimal clearance, the particle achieves approximately two regular impacts per excitation cycle with sufficient mean impact velocity, supporting the role of impact sequencing and impact velocity in the observed suppression. At non-optimal clearances, this condition breaks down, either through excessive low-momentum impacts at undersized clearances, or through infrequent high-velocity but insufficient contacts at oversized clearances, explaining the loss of modal selectivity.

Good agreement between numerical predictions and experimental measurements across frequency response, energy distribution, inter-storey drift, and time histories confirms the consistency of the modelling framework with the tested configuration. Since the model parameters were identified from the same experimental structure, this agreement validates the modelling approach for similar lightly damped shear-type configurations rather than constituting a general predictive validation. The observed robustness to impact material properties further simplifies practical implementation, as performance is governed primarily by impact dynamics rather than exact restitution or stiffness values.

Future studies could explore optimized damper placement, multi-amplitude characterization, and performance under broadband and seismic excitations. Overall, the TSPID offers a simple, cost-effective passive solution for mode-selective vibration control through geometric optimization. The demonstrated robustness to material properties, combined with the practical utility of normalized clearance as a design parameter, positions the TSPID as a practical low-cost alternative to TMDs in resonance-dominated engineering applications.

Author contributions Muhammad Ayaz Akbar: Conceptualization, Data Curation, Formal Analysis, Investigation, Methodology, Software, Validation, Visualization, Writing – Original Draft, and Writing – Review & Editing. Emiliano Rustighi: Conceptualization, Data Curation, Methodology, Validation, Visualization, Writing – Review & Editing Muhammad Gulzari: Methodology, Validation, Funding Acquisition, Project Administration, Resources, Supervision, Writing – Review & Editing Chengzhen YIN: Data Curation, Investigation, Methodology, Software, Validation, Visualization, Writing – Review & Editing Qinghua QIN: Funding Acquisition, Project Administration, Resources, Supervision, Writing – Review & Editing.

Funding The authors would like to acknowledge the financial support from National Natural Science Foundation of China (Grant No. 12272239) and University College Dublin (UCD), Output Based Research Support Scheme (OBRSS).

Data availability The dataset generated/collected during the current study are available from the corresponding authors on a reasonable request.

Declarations

Conflict of interest The authors declare that they have no conflict of interest.

References

1. Machado, M.R., Dutkiewicz, M.: Wind turbine vibration management: an integrated analysis of existing solutions, products, and open-source developments. Energy Rep. **11**, 3756–3791 (2024)
2. Huang, Z., et al.: Experimental and numerical study on concrete beams reinforced with basalt FRP bars under static and impact loads. Compos. Struct. **263**, 113648 (2021)
3. Balaji, P.S., Karthik SelvaKumar, K.: Applications of nonlinearity in passive vibration control: a review. J. Vib. Eng. & Technol. **9**(2), 183–213 (2021)
4. Wang, B.S., et al.: Experiment and numerical simulation on the performance of multiple unidirectional single-particle dampers under seismic excitation. Earthq. Eng. Struct. Dyn. **53**(6), 1982–2005 (2024)
5. Sun, H.D., et al.: Numerical simulation and dynamic experimental investigation on vibration control of a structural system with a stacked single particle-inerter damper. Earthq. Eng. Struct. Dyn. **53**(11), 3649–3677 (2024)
6. Nistri, F., et al.: Design and in field validation of a modular metamaterial for mitigation of railway induced vibrations. Soil Dyn. Earthq. Eng. (2024). https://doi.org/10.1016/j.soildyn.2024.108594
7. Koutsoloukas, L., Nikitas, N., Aristidou, P.: Passive, semi-active, active and hybrid mass dampers: a literature review with associated applications on building-like structures. Dev. Built Environ. **12**, 100094 (2022)
8. Nehemy, G.F., et al.: A passive self-tuning vibration neutraliser using nonlinear coupling between the degrees of freedom. Mech. Syst. Signal Process. **185**, 109786 (2023)
9. Roozbahan, M., Turan, G.: An improved passive tuned mass damper assisted by dual stiffness. Structures **50**, 1598–1607 (2023)
10. Wang, L., et al.: Experimental study on adaptive-passive tuned mass damper with variable stiffness for vertical human-induced vibration control. Eng. Struct. **280**, 115714 (2023)
11. Chowdhury, S., Banerjee, A., Adhikari, S.: A critical review on inertially-amplified passive vibration control devices. Arch. Comput. Methods Eng. **31**(4), 2139–2175 (2024)
12. Enríquez-Zárate, J., et al.: Passive vibration control in a civil structure: experimental results. Meas. Control **52**(7–8), 938–946 (2019)
13. Madhekar, S., Matsagar, V.: Passive vibration control of structures. CRC Press (2022)
14. Gagnon, L., Morandini, M., Ghiringhelli, G.L.: A review of particle damping modeling and testing. J. Sound Vib. **459**, 114865 (2019)
15. Liao, C.C., Chung, Y.C., Weng, C.H.: A study on the energy dissipation mechanism of dynamic mechanical systems with particle dampers by using the novel energy method. Nonlinear Dyn. **111**(17), 15955–15980 (2023)
16. Masri, S.F., et al.: Active parameter control of nonlinear vibrating structures. J. Appl. Mech. **56**(3), 658–666 (1989)
17. Masri, S.F.: General motion of impact dampers. J. Acoust. Soc. Am. **47**(1B), 229–237 (1970)
18. Masri, S.F.: Numerical response characteristics of systems provided with impact dampers. Univ., Structural Mechanics Lab, Southern California (1970)

19. Masri, S.F.: Analytical and experimental studies of multiple-unit impact dampers. J. Acoust. Soc. Am. **45**(5), 1111–1117 (1969)
20. Masri, S.F.: Effectiveness of two-particle impact dampers. J. Acoust. Soc. Am. **41**(6), 1553–1554 (1967)
21. Masri, S.F., Caughey, T.K.: On the stability of the impact damper. J. Appl. Mech. **33**(3), 586–592 (1966)
22. Nigm, M.M., Shabana, A.A.: Effect of an impact damper on a multi-degree of freedom system. J. Sound Vib. **89**(4), 541–557 (1983)
23. Saeed, A.S., Abdul Nasar, R., Al-Shudeifat, M.A.: A review on nonlinear energy sinks: designs, analysis and applications of impact and rotary types. Nonlinear Dyn. **111**(1), 1–37 (2022)
24. Bergeot, B., Bellizzi, S., Cochelin, B.: Passive suppression of helicopter ground resonance using nonlinear energy sinks attached on the helicopter blades. J. Sound Vib. **392**, 41–55 (2017)
25. Gourc, E., et al.: Quenching chatter instability in turning process with a vibro-impact nonlinear energy sink. J. Sound Vib. **355**, 392–406 (2015)
26. Xie, R., et al.: Experimental investigation of vortex-induced vibration mitigation of a long-span bridge with nonlinear energy sink inerter using real-time hybrid simulation. Eng. Struct. **357**, 122529 (2026)
27. Bapat, C.N., Sankar, S.: Single unit impact damper in free and forced vibration. J. Sound Vib. **99**(1), 85–94 (1985)
28. Duncan, M.R., Wassgren, C.R., Krousgrill, C.M.: The damping performance of a single particle impact damper. J. Sound Vib. **286**(1–2), 123–144 (2005)
29. Chehaibi, K., Mrad, C., Nasri, R.: Collision modeling of single unit impact absorber for mechanical systems vibration attenuation. J. Theor. Appl. Mech. **57**(4), 947–956 (2019)
30. Wang, Y., et al.: Prediction methods for the damping effect of multi-unit particle dampers based on the cyclic iterations of a single-unit particle damper. J. Sound Vib. **443**, 341–361 (2019)
31. Wang, B.-S., et al.: Experimental and performance analysis of the combined damping system with a TMD and a multiple unidirectional single-particle damper. J. Sound Vib. **540**, 117301 (2022)
32. Wang, B.S., et al.: Experimental and optimization analysis of a multiple unidirectional single-particle damper. J. Sound Vib. **553**, 117664 (2023)
33. Akbar, M.A., Wong, W.O., Rustighi, E.: Design optimization of a single-mass impact damper. J. Sound Vib. **570**, 118019 (2024)
34. Akbar, M.A., Wong, W., Rustighi, E.: A study of soft and hard impact effects in single-particle impact dampers. J. Vib. Control **31**(15–16), 3357–3370 (2025)
35. Rathi, A.K., Chakraborty, A.: Reliability-based performance optimization of TMD for vibration control of structures with uncertainty in parameters and excitation. Struct. Control. Health Monit. (2017). https://doi.org/10.1002/stc.1857
36. Snoun, C., Trigui, M.: Design parameters optimization of a particles impact damper. Int. J. Interact. Des. and Manuf (IJIDeM) **12**(4), 1283–1297 (2018)
37. Zhang, R., et al.: Parametrical optimization of particle dampers based on particle swarm algorithm. Appl. Acoust. **160**, 107083 (2020)
38. Guo, X., Zhu, Y., Cao, D.: Dynamic design and performance prediction of tuned particle dampers based on co-simulation. Nonlinear Dyn. **113**(4), 3053–3077 (2025)
39. Lu, Z., et al.: Particle tuned mass dampers for wind-induced vibration control in supertall building tower crowns. Int. J. Struct. Stab. Dyn. **0**, 2550209 (2024)
40. Soureshjani, O.K., Hosseini Lavassani, S.H.: Performance of tuned particle impact damper and tuned mass damper seismic control systems considering mainshock-aftershock. Structures **56**, 104924 (2023)
41. Jin, J., et al.: Railway noise reduction by periodic tuned particle impact damper with bounce and pitch-coupled vibration modes. Compos. Struct. **284**, 115230 (2022)
42. Lu, Z., Chen, X., Zhou, Y.: An equivalent method for optimization of particle tuned mass damper based on experimental parametric study. J. Sound Vib. **419**, 571–584 (2018)
43. Zalewski, R., et al.: Experimental research and modeling of soft rubber semi active vacuum packed particles torsional damper. Arch. Civ. Mech. Eng. **26**(2), 96 (2026)
44. Lu, Z., et al.: A semi-active impact damper for multi-modal vibration control under earthquake excitations. Mech. Syst. Signal Process. **210**, 111182 (2024)
45. Huang, X., et al.: Vibration reduction performance and mechanical model of circular cavity non-packed particle damper. Int. J. Struct. Stab. Dyn. **0**(0), 2750112 (2025)
46. Papalou, A.: Effects of the design configuration on the performance of compartmental particle dampers. Int. J. Civ. Eng. **20**(11), 1353–1361 (2022)
47. Huang, X.H., et al.: Equivalent model and parameter analysis of non-packed particle damper. J. Sound Vib. **491**, 115775 (2021)
48. Ni, W., et al.: An experimental investigation of modal control and suppression mechanism of particle damping on vortex induced vibration. Nonlinear Dyn. **113**(3), 2079–2090 (2025)
49. Machado, M.R., Dutkiewicz, M.: Enhancing broadband vibration suppression of a cable conductor using graded metamaterials. J. Brazilian Soc. Mech. Sci. Eng. **46**(4), 190 (2024)
50. Prasad, B.B., et al.: Design strategies of particle dampers for large-scale applications. J. Vib. Eng. & Technol. **12**(4), 5715–5746 (2024)
51. Prasad, B.B., et al.: Application of particle dampers on a scaled wind turbine generator to improve low-frequency vibro-acoustic behavior. Appl. Sci. **12**(2), 671 (2022)
52. Zhang, Z., et al.: Mitigation of edgewise vibrations in wind turbine blades by means of roller dampers. J. Sound Vib. **333**(21), 5283–5298 (2014)
53. Zhang, J., et al.: Seismic control performance of multi-story structures with an enhanced particle inerter device (EPID). Eng. Struct. (2024). https://doi.org/10.1016/j.engstruct.2024.117849
54. Shen, B.T., et al.: Seismic control of super high-rise structures with double-layer tuned particle damper. Earthq. Eng. Struct. Dyn. **50**(3), 791–810 (2021)
55. Zhao, Z., Zhang, R., Lu, Z.: A particle inerter system for structural seismic response mitigation. J. Frankl. Inst. **356**(14), 7669–7688 (2019)
56. Li, K., Darby, A.P.: Experiments on the effect of an impact damper on a multiple-degree-of-freedom system. J. Vib. Control **12**(5), 445–464 (2016)
57. Li, K., Darby, A.P.: Modelling a buffered impact damper system using a spring-damper model of impact. Struct. Control. Health Monit. **16**(3), 287–302 (2009)
58. Li, K., Darby, A.P.: A buffered impact damper for multi-degree-of-freedom structural control. Earthq. Eng. Struct. Dyn. **37**(13), 1491–1510 (2008)
59. Li, K., Darby, A.P.: An experimental investigation into the use of a buffered impact damper. J. Sound Vib. **291**(3–5), 844–860 (2006)
60. Geng, X., et al.: Suppression of multiple modal resonances of a cantilever beam by an impact damper. Appl. Math. Mech. **41**(3), 383–400 (2020)
61. Masri, S.F., Caffrey, J.P.: Response of a multi-degree-of-freedom system with a pounding vibration neutralizer to harmonic and random excitation. J. Sound Vib. **481**, 115427 (2020)
62. Akbar, M.A., Wong, W.-O., Rustighi, E.: A hybrid damper with tunable particle impact damping and Coulomb friction. Machines **11**(5), 545 (2023)
63. Duncan, M.R., Wassgren, C.R., Krousgrill, C.M.: The damping performance of a single particle impact damper. J. Sound Vib. **286**(1), 123–144 (2005)
64. Li, X., et al.: Irreversible energy transfers in systems with particle impact dampers. Nonlinear Dyn. **112**(1), 35–58 (2024)

65. Park, K.C., Underwood, P.G.: A variable-step central difference method for structural dynamics analysis — part 1. Theoretical aspects. Comput. Methods Appl. Mech. Eng. **22**(2), 241–258 (1980)
66. To, C.W.S.: The stochastic central difference method in structural dynamics. Comput. Struct. **23**(6), 813–818 (1986)
67. Soares, D., Großeholz, G.: Nonlinear structural dynamic analysis by a stabilized central difference method. Eng. Struct. **173**, 383–392 (2018)
68. Wu, B., et al.: Stability and accuracy analysis of the central difference method for real-time substructure testing. Earthq. Eng. Struct. Dyn. **34**(7), 705–718 (2005)
69. Engineers, A.S.o.C.: Minimum design loads and associated criteria for buildings and other structures. American Society of Civil Engineers (2022)
70. Standard, B.: Eurocode 8: design of structures for earthquake resistance. Part **1**, 1998–2001 (2005)
71. Lu, Z., et al.: Shaking table test of the effects of multi-unit particle dampers attached to an MDOF system under earthquake excitation. Earthq. Eng. Struct. Dyn. **41**(5), 987–1000 (2012)
72. Lu, Z., et al.: Experimental studies of the effects of buffered particle dampers attached to a multi-degree-of-freedom system under dynamic loads. J. Sound Vib. **331**(9), 2007–2022 (2012)

Publisher's Note Springer Nature remains neutral with regard to jurisdictional claims in published maps and institutional affiliations.

Springer Nature or its licensor (e.g. a society or other partner) holds exclusive rights to this article under a publishing agreement with the author(s) or other rightsholder(s); author self-archiving of the accepted manuscript version of this article is solely governed by the terms of such publishing agreement and applicable law.